Worcester Polytechnic Institute
Digital WPI

Major Qualifying Projects (All Years) | Major Qualifying Projects

April 2018

Bio-alcohol Extraction with Supercritical Carbon Dioxide

John Frigo
Worcester Polytechnic Institute

Follow this and additional works at: https://digitalcommons.wpi.edu/mqp-all

Repository Citation
Frigo, J. (2018). Bio-alcohol Extraction with Supercritical Carbon Dioxide. Retrieved from https://digitalcommons.wpi.edu/mqp-all/1984

This Unrestricted is brought to you for free and open access by the Major Qualifying Projects at Digital WPI. It has been accepted for inclusion in Major Qualifying Projects (All Years) by an authorized administrator of Digital WPI. For more information, please contact digitalwpi@wpi.edu.

Bio-alcohol Extraction with Supercritical Carbon Dioxide

A Major Qualifying Project submitted to the faculty of the Chemical Engineering Department at WORCESTER POLYTECHNIC INSTITUTE in partial fulfillment of the requirements for the degree of Bachelor of Science.

Submitted by:

John Frigo

Project Advisor: Professor Michael Timko

Abstract

The depletion of fossil fuels along with the growing population and energy consumption is leading researchers to look at biofuels as renewable resources. Currently ethanol is the most commonly used biofuel, but longer chain bio-alcohols like butanol offer a higher energy density, which is a promising replacement. Butanol's potential as a biofuel is limited by the current ability to produce and recover it. Difficulties lie in traditional recovery methods like distillation. A favorable replacement to this is using supercritical carbon dioxide to extract butanol from an aqueous solution. This method is primarily used for small scale extractions and to increase its viability, proper models are necessary to scale-up. Understanding mass transport limitations are key to scale-up and there is a proposed model for the volumetric mass transfer coefficient $k_l a$. This project substantiates that prediction for $k_l a$ by fitting correlations for $k_l a$ to the values that the model predicts. This comparison of model and correlations confirmed the accuracy of the model as a predictor of mass transfer coefficients in supercritical fluid extraction.

Table of Contents

Acknowledgements

I would like to thank my advisor Professor Timko for his continual support of this project as well as Professor Tompsett for his help and availability for this project.

Chapter 1: Introduction

The exponential growth of the human population coupled with a similar growth in technology has presented the parallel need for an ever increasing supply of energy. Traditionally, we have relied on burning fossil fuels, but their non-renewability and adverse impact on the environment is causing us to look for different methods to supply our need for energy. Petroleum and coal are two of the prominent sources of energy that the world relies on, but each fossil fuel has a downside. Petroleum is simply running out, and by some estimates, will only be sufficient for the world's energy consumption until the year 2030 (Shafiee & Topal, 2009). Coal, is rather abundant and makes up about 65% of the world's fossil fuel reserves, but it has detrimental effects on the environment (Shafiee & Topal, 2009). Coal fired power plants produce vastly more air pollutants than other industry pollution sources (American Lung Association National Headquarters Offices, 2011). These limitations are causing us to look at alternative energy sources such as solar power, nuclear power, and biofuels.

As natural resources are depleted, biofuels will become a major energy source over the next hundred years (Shafiee & Topal, 2009). One of the most commonly used biofuels is ethanol. It is produced by fermenting starches and sugars, though there is research being done to obtain ethanol from cellulose. The primary use of ethanol is as a blending agent, in which it is mixed with gasoline, cutting down on carbon monoxide emissions and other pollutants (National Renewable Energy Laboratory). Despite ethanol's common use in vehicles, the organic molecule has a low energy density compared to higher carbon chain molecules. Ethanol has a lower heating value (LHV) of 76,000 BTU/gal in contrast with gasoline's LHV of 112,000 BTU/gal (*Fuel Properties Comparison*, 2014). There are higher chain bio-alcohols more suited to mixing with gasoline, such as butanol which contains 30% more energy than ethanol (Qureshi, 2010).

Butanol is commonly produced through acetone butanol ethanol (ABE) fermentation. The process can use a variety of sugars such as lactose, sucrose, glucose, fructose, mannose, dextrin, starch, and others (Qureshi, 2010). This produces a mixture of acetone, butanol and ethanol in a 3:6:1 ratio respectively. ABE fermentation is a well-practiced method of producing butanol and has been in use for around a century, but butanol's potential is limited by the difficulty of separating it from its aqueous solution. Butanol and water form an azeotrope that makes separation

by distillation difficult (Luyben, 2008). Because of this, it has been necessary to seek alternative methods of separation, particularly gas stripping.

Gas stripping presents its own difficulties, but fortunately, a bacteria strain was discovered that helps to overcome obstacles of the operation. *Bacillus Megaterium* SR7 is able to survive and produce butanol at high pressures of 100 bar (Thompson et al., 2016). This high pressure allows for the use of supercritical carbon dioxide as a stripping agent. At this pressure and higher temperatures, CO_2 is past its critical point, offering several unique advantages. The first is that CO_2 is inflammable, nontoxic and relatively inexpensive. Additionally, the recovery of butanol after extraction with supercritical CO_2 requires only a simple pressure drop to return CO_2 to its gaseous state (Moreno et al., 2014). Though promising, supercritical fluid extraction (SFE) faces the difficulty of scale-up to be feasible.

Currently, SFE is primarily done on a small scale and there is no standard for scale up of the process, presenting a difficulty in using butanol as a viable biofuel. There are high manufacturing costs involved in the process due to the energy required to achieve the high pressures for achieving the supercritical state (Rosa & Meireles, 2005). For scale-up of the SFE process, solubility and the mass transfer behavior needs to be understood (Özkal, 2005). This project examines a proposed model for mass transfer behavior to corroborate it. To inspect and analyze this model, it is compared to established correlations for the mass transfer coefficient and to experimental data of these mass transfer coefficients.

Chapter 2: Background

2.1 Biofuels

2.1.1. Energy Consumption

The world consumed over 92 million barrels of oil a day in 2016 and this consumption rate has only increased throughout history and is predicted to continue the trend (BP, 2017). From 2015 to 2016 world oil consumption increased by 1.6%, while world energy production only increased 0.5% in the same timeframe (BP, 2017). Oil is the leading energy source in North America, South America, Africa, and still a prominent source on the other continents (BP 2017). Oil is primarily refined to gasoline and to diesel fuel in the United States, the largest petroleum consumer (EIA, 2017). It makes up almost 18% of the fossil fuel reserves (Shafiee & Topal, 2009).

Total energy consumption grew by 1.0% in 2016 and over the past 10 years has grown an average of 1.8% per year (BP, 2017). This gradual increase paired with the world's use of primarily non-renewable resources is bound for an energy shortage in the near future. There are several estimates of when these non-renewable sources will be expended, but one estimate predicts that by 2030, the oil production will no longer be sufficient for the world's energy consumption (Shafiee & Topal, 2009). Thus there is a need for a reasonable substitute. Coal makes up about 65% of the world's energy reserves, but the environmental problems with coal prevent it from expanding as a fossil fuel (Shafiee & Topal, 2009). Natural gas is another fossil fuel that accounts for a large portion of energy consumption, but similar to oil makes up only 17% of fossil fuel reserves (Shafiee & Topal, 2009). A recognizable energy shortage is forthcoming, and we have resultantly looked to using more renewable energy sources.

2.1.2 Renewable Energy

In 2016, renewable energy accounted for 14.5% of the world's energy consumption, including nuclear energy, hydroelectricity, wind, geothermal, solar, biomass and waste. This was a 14.1% growth over the year and indicative of the shift towards cleaner energy (BP, 2017). This shift is beneficial to the environment as renewable energies are more carbon neutral (Earley & McKeown). Biofuels are a bioenergy derived from biomass and is of particular interest because it can be mixed with gasoline for motor vehicles (Earley & McKeown). Mixing biofuels with

gasoline presents the advantage of lowering carbon emissions and reducing the expenditure of non-renewable resources (Earley & McKeown).

Ethanol is most commonly blended with gasoline in the United States to reduce carbon monoxide and smog-causing pollutants. Ethanol has oxygen and it acts as an oxygenate when mixed with gasoline (*Oxygenates Fact Book*). Oxygenates increase the oxygen content in gasoline which allows for more complete fuel combustion. This complete combustion then leads to the reduction of carbon monoxide in the winter, smog-causing pollutants in the summer and the reduction of toxic emissions year round (*Oxygenates Fact Book*). Bio-ethanol though practical and commonly used is not the ideal candidate for blending with gasoline and other longer carbon chain molecules like bio-butanol present benefits not found in ethanol.

2.1.3 Ethanol and Butanol Comparison

Both ethanol and butanol offer unique advantages in their use as a biofuel. As they both serve to blend with gasoline, their benefits must be compared in relation to how they function with gasoline. Butanol is a 4-carbon alcohol compared to the 2-carbon ethanol, providing butanol with a higher energy density, making it more suited for mixing with gasoline (Alternative Fuels Data Center, n.d.). Ethanol has a lower heating value (LHV) of 76,000 BTU/gal compared to gasoline at 112,000 BTU/gal (Fuel Properties Comparison, 2014). The LHV describes the amount of heat released in combustion to do work subtracting the heat of vaporization of the water byproducts. The LHV for ethanol is 37% lower than gasoline, while butanol's LHV is only 22.5% less than gasoline (Wallner et al., 2009). Octane number is another consideration in contrasting the two biofuels. Gasoline and butanol have similar octane ratings, at 90 and 87 respectively, compared to the higher octane rating of ethanol at 100 (Wallner et al., 2009). Additionally, ethanol is fully miscible in water, so it cannot be transported by a pipeline like gasoline. Butanol is considerably less soluble in water and can be transported by pipeline with gasoline (Wallner et al., 2009).

Despite butanol's distinct advantages, ethanol is still widely used as a biofuel. This is due to the difficulty and high costs of producing and separating butanol. Butanol forms a heterogeneous azeotrope with water, making the distillation of butanol difficult. The azeotrope occurs in the decanter and a simple two column distillation process cannot be used (Luyben, 2008). This drives the cost and is one of the reasons butanol is not commonly used as a blending agent in gasoline.

Other recovery methods such as gas stripping are being pursued in an attempt to make butanol more viable.

2.1.4 Bio-butanol Production

Butanol is produced by fermenting biomass similarly to the production of ethanol. The process is called ABE fermentation and generates acetone, butanol and ethanol in a 3:6:1 ratio respectively (Qureshi, 2010). ABE fermentation can utilize a variety of sugars such as lactose, sucrose, glucose, fructose, mannose, dextrin, starch, and others (Qureshi, 2010). A promising new bacteria strain *Bacillus megaterium* SR7 was recently discovered which can be modified to produce bio-alcohols (Thompson et al., 2016). This strain is especially integral to butanol because of its survivability in high pressure, low pH and anaerobic conditions (Thompson et al., 2016). This makes *B. megaterium* and ideal candidate for supercritical fluid extraction and offers a potential new method for butanol extraction that bypasses the difficulties of distillation.

2.2 Supercritical Fluid Extraction

Supercritical fluid extraction utilizes a solvent above its critical point to extract a solute (Seader & Henley, 1998). Solute extraction in general requires two steps, the initial extraction and then a separation of the solute and solvent (Seader & Henley, 1998). With supercritical fluids, this second step is simple and only requires a pressure drop to return the supercritical fluid to its gaseous state resulting in an effective separation of solvent and solute (Moreno et al., 2014).

2.2.1 Supercritical Carbon Dioxide

Carbon Dioxide is a commonly used solvent for SFE. It is relatively safe because it is non-toxic and non-flammable, while also being cost effective (Özkal, 2004). Its critical point is 304.2 K and 73.8 bar and above this temperature, carbon dioxide enters the supercritical phase (Suehiro et al., 1996). Figure 1 below depicts a phase diagram for CO_2.

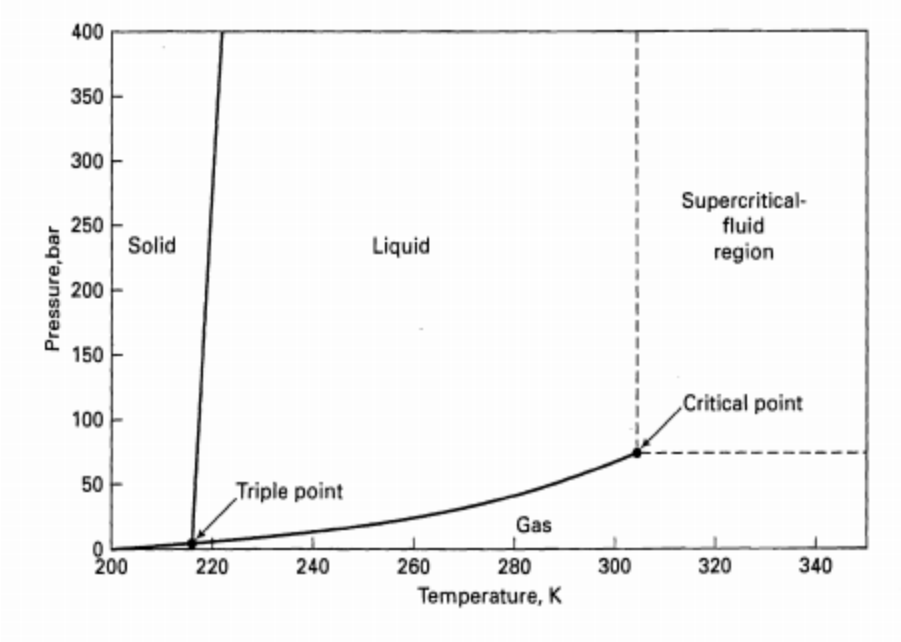

Figure 1: CO_2 Phase Diagram (Seader &Henley, 1998)

Carbon dioxide is especially suited for butanol extraction. High molecular weight alcohols are less miscible in water and less volatile than lower weight alcohols which. This is an indication of carbon dioxide's potential as a better solvent for extracting from aqueous solutions because distribution coefficients are more favorable for more hydrophobic alcohols (Laitinen & Kaunisto, 1999).

2.2.2 Advantages and Disadvantages of SFE

Due to some unique properties, supercritical fluids are excellent solvents. As pressure increases closer towards the critical point and beyond the critical point, the pressurized solvent drastically increases solubility of a solute (Seader & Henley, 1998). This phenomenon is due to the density increase as its reciprocal specific volume decreases with pressure. As an example, ethylene at 2 MPa has a density of 25.8 g/L and a solubility of p-iodochlorobenzene (pICB) of 0.015 g/L. When pressurized above the critical point to 8 MPa, the density increases to 267 g/L and has a solubility of pICB of 40 g/L which is 2,700 times higher than the solubility at subcritical pressure (Seader & Henley, 1998). In addition, for near critical fluids, the diffusivity of solute molecule is one to two orders of magnitude higher than in a normal solvent, resulting in lower mass transfer resistance (Seader & Henley, 1998). Finally, the viscosity of supercritical fluids is lower than normal fluids, again improving the solubility in the solvent (Seader & Henley, 1998).

SFE offers high extraction rates, but the process has high costs due to high costs for solvent pressurization to reach critical pressures (Seader & Henley, 1998). It is often used for small scale extraction of large, relatively non-volatile solutes in solid or liquid mixtures (Seader & Henley, 1998). This poses a problem for extracting butanol to be used as a major biofuel. Currently, there is no standard for scale up of the SFE process (Rosa & Meireles, 2005). Developing this method of scale-up requires the understanding of solubility and mass transfer behavior (Özkal, 2004).

2.2.3 SFE Scale-Up Research

With these complications, WPI is doing research to overcome difficulties in scaling up the butanol production. Models of equilibrium and mass transport behavior are being developed using data from a pilot semi-batch supercritical fluid extraction unit. Figure 2 below depicts a model of the pilot vessel created by Tom Partington of the WPI Chemical Engineering Department.

Figure 2: Pilot Extraction Vessel Model

These models are expected to be used in the scale up of bio-butanol production and extraction.

2.3 Modeling supercritical fluid extraction of alcohols

2.3.1 Mass Transfer and Thermodynamic Limitations

It is key to be able to understand and model the mass transfer in $scCO_2$ extraction at high flow rates for scaling up SFE of alcohols. Experiments for a semi-batch extraction vessel were run at WPI to obtain data for developing a method to predict the behavior of alcohols in the SFE process. The difficulty in developing this model is that both thermodynamics and mass transport factors influence the data. Thus the method to understand the extraction data must account for the mass transport factors as well as the thermodynamic factors. These two limitations have distinct regimes where each determines the behavior of the extraction. Figure 3 below depicts the regimes for mass transfer and equilibrium limitations (DiSpirito & Stolz, 2017).

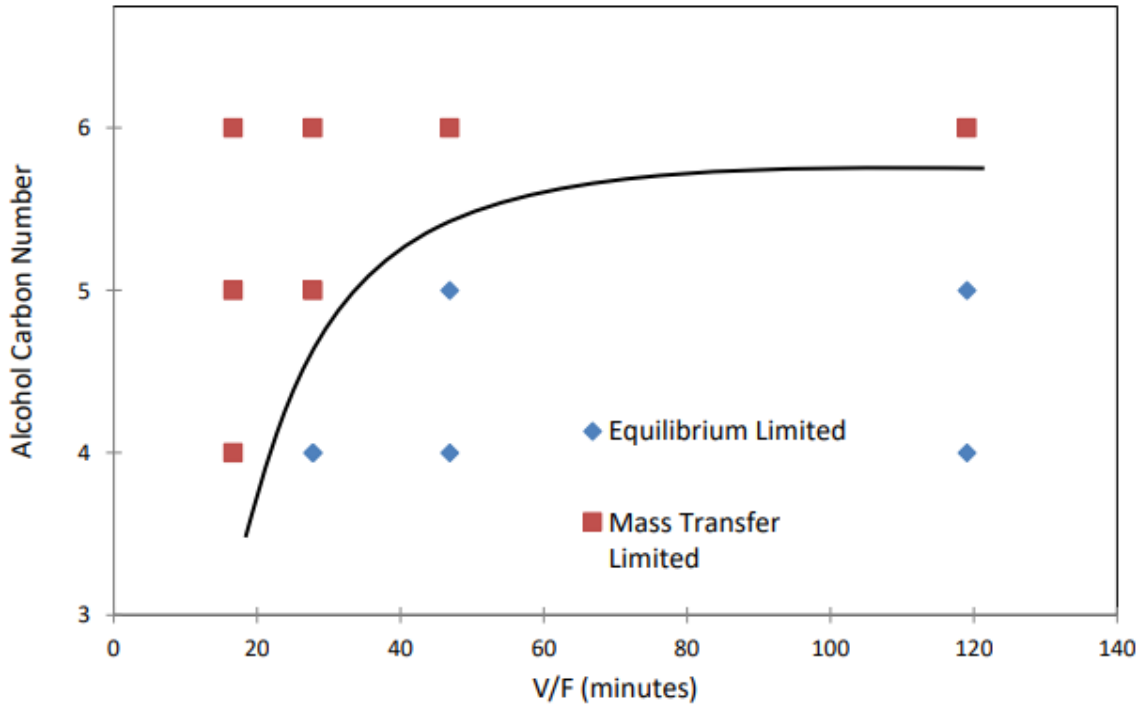

Figure 3: A comparison of conditions where alcohol extraction is equilibrium or mass transfer limited (DiSpirito & Stolz, 2017)

At a constant volume, the volumetric flow rate of CO_2 is the determining factor for the extraction regime. At lower CO_2 flow rates, the system is equilibrium limited while at higher flow rates the system is mass transfer limited. Additionally, for longer carbon chains the system is pushed into the mass transfer limited regime (DiSpirito & Stolz, 2017). Diffusivity of solvents tends to decrease as molar volume is increased or chain length is extended, likely resulting in this

phenomenon (Wankat, 2012). Understanding the limitations on extraction allows a model to be developed.

2.3.2 Mathematical Modeling

The semi-batch vessel used to obtain data can be modeled mathematically. For the internally mixed system, the mass balance equations are:

$$\frac{V_C}{V_W}\frac{dC_C}{dt} = -\frac{Q_C C_C}{V_W} + k_l a\left(K_{C/W} C_W - C_C\right) \quad (1)$$

$$\frac{dC_W}{dt} = -k_l a\left(K_{C/W} C_W - C_C\right) \quad (2)$$

Where $k_l a$ is the mass transfer coefficient multiplied by the interfacial area; *Vc/Vw* is the ratio of hold-up volumes of CO_2 and water; Q_c is the volumetric CO_2 flow rate; *Cc* and *Cw* are the time-dependent concentrations of alcohol in the gas and liquid phases; and $K_{C/W}$ is the equilibrium coefficient that governs the equilibrium distribution of alcohol between $scCO_2$ and water phases (Tompsett et al., intended for submission). The initial conditions are:

$$C_W(t = 0) = C_{W.o} \quad (3)$$

$$C_C(t = 0) = 0 \quad (4)$$

The equations can be non-dimensionalized with:

$$Pe = \frac{Q_C}{V_W k_l a} \quad (5)$$

$$\theta_W = \frac{C_W}{C_{w,o}} \quad (6)$$

$$\tau = t\, k_l a \quad (7)$$

$$\theta_C = \frac{C_C}{K_{C/W} C_{w,o}} \quad (8)$$

Where Pe is the Péclet number, which is the ratio of the rate of advective transport to the rate of diffusional transport. Vc/Vw can be redefined as $\emptyset$ (Tompsett et al., intended for submission). Equation (1) and (2) become:

$$\phi \frac{d\theta_C}{d\tau} = -Pe\ \theta_C + (\theta_W - \theta_C) \quad (9)$$

$$\frac{d\theta_W}{d\tau} = -\ K_{C/W}\ (\theta_W - \theta_C) \quad (10)$$

When *Pe = 0*, diffusional transport is the limiting factor, equations (9) and (10) follow the constraint $\phi K_{C/W}\theta_c + \theta_w = 1$, and the full solution becomes:

$$\theta_c(\tau) = \frac{1}{1+\phi K_{C/W}}\left(1 - e^{-\frac{1+\phi K_{C/W}}{\phi}\tau}\right) \quad (11)$$

$$\theta_w(\tau) = \frac{1}{1+\phi K_{C/W}}\left(1 + \phi K_{C/W}\, e^{-\frac{1+\phi K_{C/W}}{\phi}\tau}\right) \quad (12)$$

For nonzero values of *Pe*, there are two decay rates as compared to the *Pe* = 0 solution with only one decay rate. $\lambda_{\pm}$ denotes the decay rates:

$$\lambda_{\pm} = -\frac{1+\phi K_{C/W}+Pe}{2\phi} \pm \frac{1}{2\phi}\sqrt{\left(1+Pe+\phi K_{C/W}\right)^2 - \phi K_{C/W}\, Pe} \quad (13)$$

Where λ_+ relates to the advection rate. The solution for Pe = nonzero is:

$$\theta_C = \frac{1}{\phi(\lambda_+ - \lambda_-)}\left\{e^{\lambda_+\tau} - e^{\lambda_-\tau}\right\} \quad (14)$$

$$\theta_W = \frac{1}{\phi(\lambda_+ - \lambda_-)}\left\{\alpha_+ e^{\lambda_+\tau} - \alpha_- e^{\lambda_-\tau}\right\} \quad (15)$$

$$\alpha_{\pm} = \phi\,\lambda_{\pm} + 1 + Pe \quad . \quad (16)$$

Choosing λ_1 as the positive root of the equation and taking the natural log of both sides of equation (15) gives:

$$\ln\theta_W = \ln\left\{\frac{\lambda_2 + \frac{K_{C/W}}{Pe}}{\lambda_2 - \lambda_1}\right\} + \lambda_1\tau \quad (17)$$

And ln θ_W graphed as a function of time has a slope of λ_1. These equations model the mass and diffusional transport for the semi-batch extraction vessel. This analysis is intended to be used to scale up the extraction process (Tompsett et al., intended for submission).

Chapter 3: Methods

3.1 Objectives

This project examines the above mathematical framework for interpreting the semi-batch data of the extraction vessel at WPI. Primarily the model for mass transport behavior is examined. The objectives of the project are:

1. Verify the assumptions made by the mathematical analysis of the extraction vessel.
2. Determine $k_l a$ for n-butanol, n-pentanol, and n-hexanol at increasing flow rates.
3. Calculate $k_l a$ for n-butanol, n-pentanol, and n-hexanol using existing correlations at the same condtions as the semi-batch pilot extraction vessel.
4. Compare the predicted and correlated values of $k_l a$ to analyze the validity of the prediction.

3.2 Numerical Verification of Assumptions

The mathematical analysis above in section 2.3.2 makes two assumptions that require verification. The first assumption is for all reasonable values of *Pe*. The mathematical analysis assumes that for typical semi-batch conditions, the absolute value of λ_+ is much less than the absolute value of λ_-. Both variables are determined from equation (13) above. To check the validity, a spreadsheet with Pe varying from 0.01 to 100 and with experimental $K_{C/W}$ values was created to solve for λ_- and λ_+. The goal of this was to determine any instances where λ_+ / λ_- approached or exceeded 1.

3.3 Confirming $k_l a$ Models

3.3.1 Calculating $k_l a$

The mathematical analysis presents two methods of predicting $k_l a$. The overall mass transfer coefficient can be determined from both the diffusion limited and mass transport limited equations with varying levels of usefulness. Equations (12) and (15) are the diffusion transport and mass transport respectively. The mass transfer coefficient was determined for increasing $scCO_2$ flow rates as demonstrated in Table 1 below

Table 1: Parameters for $k_l a$ calculation				
Alcohol	Flow rate of CO_2 (ml/min)			
n-butanol	1.3	3.2	5.4	9
n-pentanol	1.3	3.2	5.4	9
n-hexanol	1.3	3.2	5.4	9

Both methods of calculation utilize the slope of the plot ln θ_W vs time which was obtained from previous experiments on the pilot vessel. Equation (12) uses $K_{C/W}$ values obtained experimentally with the same pilot vessel to calculate values of $k_l a$.

3.3.2 Comparing to Existing $k_l a$ Correlations

With predicted values of the overall mass transfer coefficient, it is important to know how these values line up with existing correlations. This project researched and examined some of these existing correlations to compare to the proposed models. The conditions of the semi-batch extraction vessel experiments were imposed on the correlations to accurately determine the closeness of predicted $k_l a$ to the correlation models. The predicted data points were curve fit to different correlations. Finally, parity plots of the predicted $k_l a$ and correlated $k_l a$ showed the accuracy of predictions to the established correlations.

Chapter 4: Results

4.1 Numerical Verification of Mathematical Assumptions

The mathematical framework makes the statement that the absolute value of λ_+ is much less than the absolute value of λ_-. For the lambda ratio verification, a numerical analysis was done for reasonable $K_{C/W}$ values and for all accessible Péclet numbers. This statement i the numerical analysis shows in Figure 4 below.

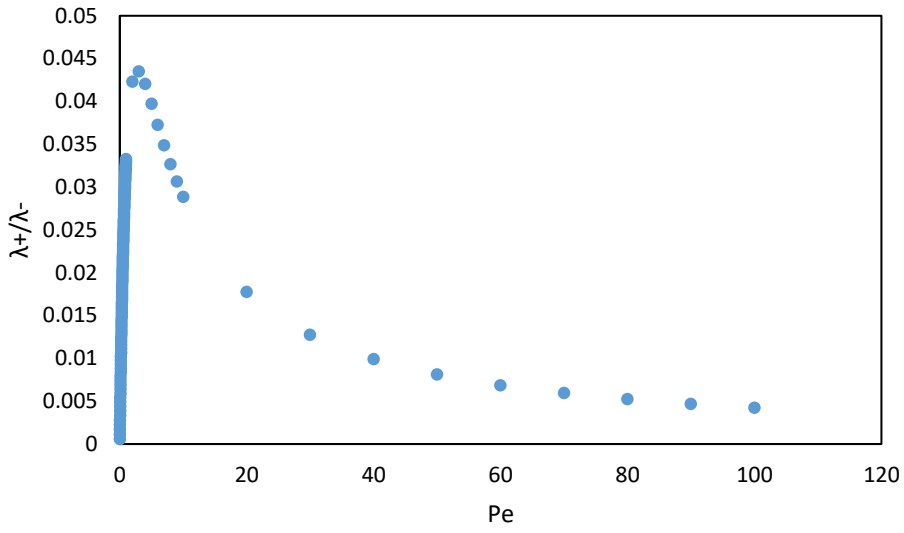

Figure 4: Lambda ratio at increasing Peclet numbers for $K_{C/W}$ = 1.57

For all accessible values of Peclet, the ratio of lambdas never goes higher than 5%. The graph in Figure 4 analyzes lambda ratios for $K_{C/W}$ = 1.57, which generated the highest ratio. At other $K_{C/W}$ values, the graphs shared the same trend, but with lower ratios, none of which exceeded 5%. This validates the statement in the mathematical framework as of λ_+ is much less than the absolute value of λ_- for all accessible Péclet values. This confirms that λ_- is the observable decay rate for small Péclet.

4.2 Predicted Values of $k_l a$

This project examines both the simple diffusion limited solution and the complex mass transport solution for $k_l a$. Both models showed data on the same order of magnitude. This 10^{-4} magnitude is expected for $k_l a$ calculated for the semi-batch pilot vessel based on a previous model

for the same vessel (DiSpirito & Stolz, 2017). Figure 5 below depicts the simple solution for $k_l a$ for n-butanol, n-pentanol, and n-hexanol.

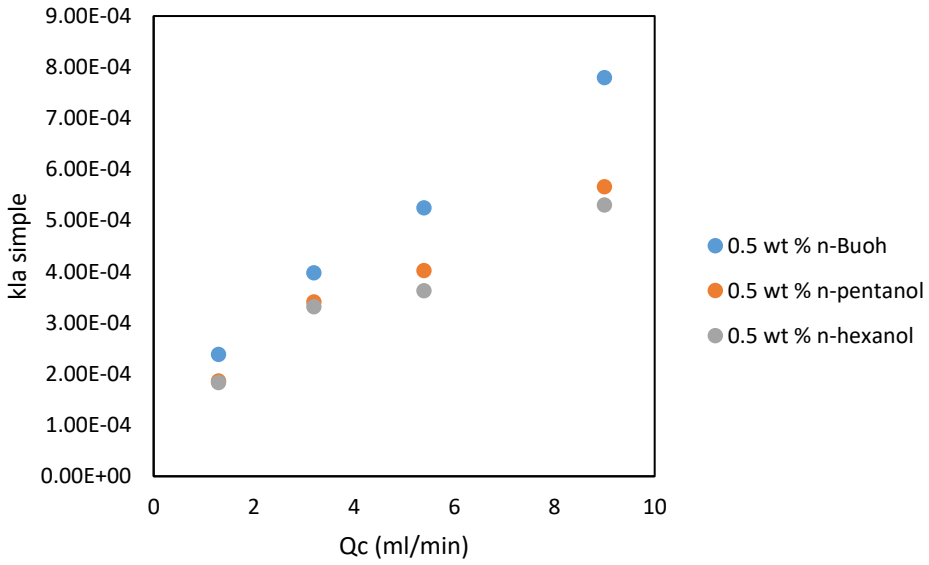

Figure 5: Simple model of the mass transfer coefficient for n-butanol, n-pentanol, and n-hexanol at increasing $scCO_2$ flow rates

The model predicts a general upwards trend in $k_l a$ as the gas flow rate increases. This is an expected trend as an increase in gas flow rate leads to an increase in interfacial area. Interfacial area a is multiplied directly by the liquid phase mass transfer coefficient k_l to get $k_l a$ so an increase in interfacial area directly leads to an increase in the overall mass transfer coefficient (Tai & Wu, 2005). Both simple and complex models predict this trend, which offers some indication a good model. Figure 6 below shows this same trend for the complex model.

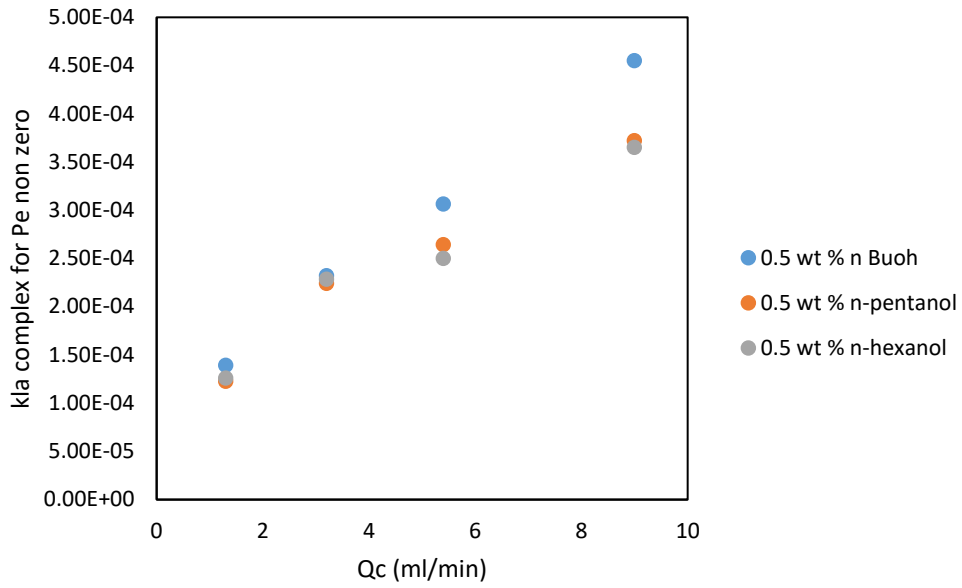

Figure 6: Complex model of the mass transfer coefficient for n-butanol, n-pentanol, and n-hexanol at increasing $scCO_2$ flow rates

The simple and complex models both demonstrate higher $k_l a$ values for butanol than hexanol and pentanol. Theory predicts that longer alcohols will have higher $k_l a$ because as the ratio of carbon-carbon bonds to hydroxyl groups increases, hydrophilicity decreases and the molecule will have more of an affinity for $scCO_2$ (Tai & Wu, 2005). The predictive models describe the opposite phenomenon and this is particularly evident for the simple calculation at high flow rates. The complex model more closely aligns with the theoretical predictions, further evidencing the accuracy of the complex model. Figure 7 below shows a comparison of the two models for n-butanol. Additionally, charts comparing the models for n-pentanol and n-hexanol are found in Appendix A. These charts depict the same trend as Figure 7.

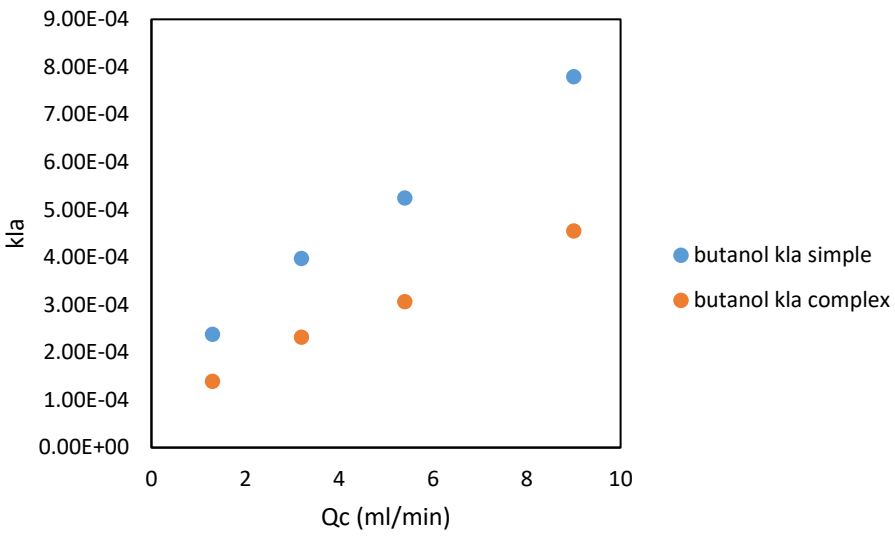

Figure 7: A comparison of complex and simple models for $k_l a$ of butanol at increasing $scCO_2$ flow rates

The chart shows the same trend for both $k_l a$ models, though the complex model predicts lower $k_l a$ values. The complex model is termed the mass transport limited solution and is thus a more accurate prediction of mass transport coefficients. In addition, this project examines experimentally obtained $k_l a$ values of ethanol at increasing flow rates from Tai & Wu. Similar to this project, their experiment utilized $scCO_2$ to extract a bio-alcohol. Figure 8 displays this comparison of complex predicted $k_l a$ values for n-butanol, n-pentanol, n-hexanol, and the experimental ethanol $k_l a$.

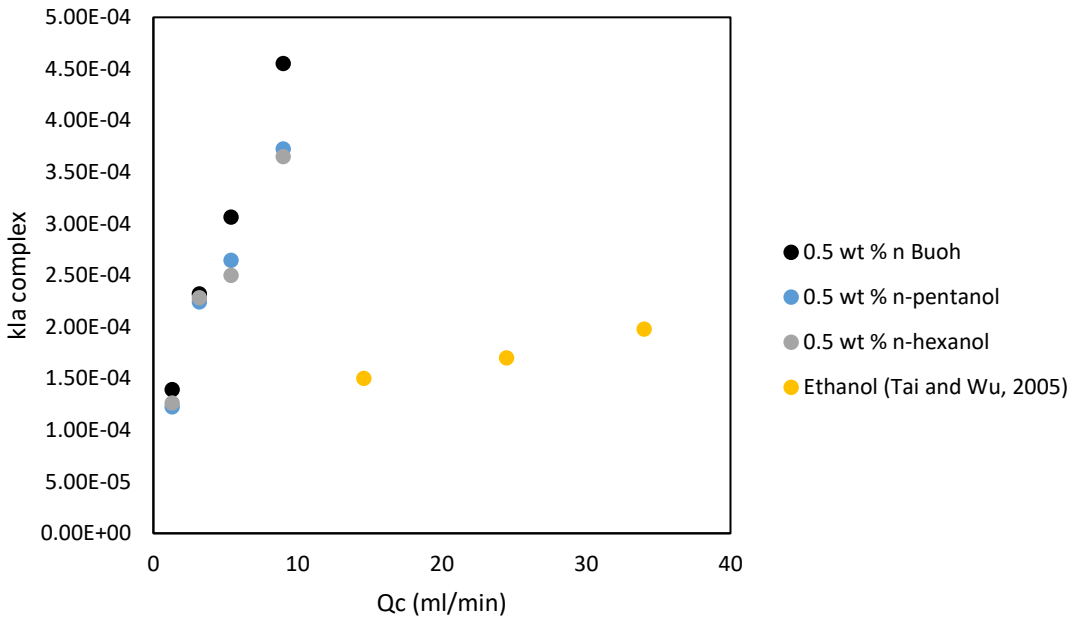

Figure 8: Mass transfer coefficients of n-butanol, n-pentanol, n-hexanol and ethanol at increasing scCO2 flow rates

The data shows a distant similarity between experimental ethanol k_la trends and the other alcohols' k_la values. The overall trend of increasing k_la with increasing $scCO_2$ flow rates is evident, but ethanol k_la values are considerably lower. Theory predicts lower k_la values for smaller chain alcohols, but the ethanol k_la is drastically different from the other alcohols. This is likely the result of different experimental conditions. Tai and Wu obtained their data in a different extraction vessel than the one at WPI. Their vessel is 7.6 cm in diameter and 28.5 cm in height compared to WPI's vessel which is 5 cm in diameter and 16.5 cm in height. The impeller is also different in Tai's experiments (Tai et al., 2000). Comparing mass transfer coefficients determined at different conditions is difficult, but the difference in magnitude of the mass transfer coefficient does not discredit the models. The similarities in trends still reinforce the model.

4.3 Comparing Predicted k_la Values with Correlations of k_la

To further corroborate the model for k_la at increasing $scCO_2$ flow rates, this project examines existing correlations for k_la at increasing $scCO_2$ flow rates to compare to the theoretical model. Numerous correlations were considered, but a large number of correlations were ruled out numerically.

4.3.1 Selection of Correlations

Choosing appropriate correlations primarily included numerically solving researched potential correlations and comparing the orders of magnitude with the predicted values of *kla*. Many of the correlations were for the liquid phase diffusion coefficient k_l, so a correlation was necessary for the interfacial area *a*. Table 2 below depicts several correlations for *a*, compiled by Painmanakul.

Table 2: A selection of interfacial area correlations (Painmanakul et al., 2009)

Eq.	Correlation	Reference
a-1	$a = \frac{6}{2.5}.(\frac{\sigma_L}{\rho_L.g})^{-0.5}.(\frac{\mu_L.U_G}{\sigma_L})^{0.25}.(\frac{\rho_L.\sigma_L^3}{g.\mu_L^4})^{0.125}.\varepsilon_G$	Van dierendonck et al. [38]
a-2	$a = 4.65 * 10^{-12} * (\frac{U_G}{\mu_L})^{0.51}$	Tomida et al. [39]
a-3	$a = \frac{6\varepsilon_G}{d_B(1-\varepsilon_G)}$	Moustiri [40]

Eq.	Correlation	Reference
ε_G -1	$\varepsilon_G = \frac{U_G}{0.3+2.U_G}$	Joshi and Sharma [41]
ε_G -2	$\varepsilon_G = \frac{U_G}{31+\beta.(1-e).\sqrt{U_G}}$ $\beta = 4.5-3.5.\exp(-0.064.d_B^{1.3})$ $e = -0.18.U_G^{1.8}/\beta$	Joshi and Shah [42]
ε_G -3	$\varepsilon_G = 0.91.U_G^{1.19}/\sqrt{g.d_B}$	Winkler [44]

To ensure accurate results, each ε_G correlation was combined with each *a* correlation for each alcohol. Table 3 numerically shows each combination for n-butanol and Appendix B displays the same numerical evaluation of interfacial area for pentanol and hexanol.

Table 3: Interfacial Area Calculations for n-Butanol				
Q cm3/s	eg 1	a3	a2	a1
0.021666667	0.003651389	0.045473	0.600275197	1.77E-11
0.053333333	0.008893116	0.138724	1.496446503	2.81E-11
0.09	0.014825843	0.263589	2.536173573	3.67E-11
0.15	0.024230749	0.489482	4.227944619	4.76E-11
Q cm3/s	eg 2	a3	a2	a1
0.021666667	3.5555E-05	0.000443	0.005823984	1.77291E-11
0.053333333	8.74629E-05	0.001364	0.014587799	2.80673E-11
0.09	0.000147514	0.002623	0.024863985	3.66518E-11
0.15	0.00024569	0.004963	0.04184117	4.75596E-11
Q cm3/s	eg 3	a3	a2	a1
0.021666667	4.59613E-05	0.000572	0.007528623	1.77291E-11
0.053333333	0.000135469	0.002113	0.022595737	2.80673E-11
0.09	0.000253824	0.004513	0.042787344	3.66518E-11
0.15	0.000468545	0.009465	0.079811245	4.75596E-11

Combining each of these correlations with correlations for k_l allowed for a complete numerical analysis of the most ideal correlation as seen in Table 4 below.

Table 4: Selected correlations for k_l		
Conditions of equation	Correlation	Source
200<Re<4000	$Sh = 0.82Re^{1/2}Sc^{1/3}$	Rowe
100<Re<1000	$Sh = 1.13\left(1 - \frac{2.9}{Re^{\frac{1}{2}}}\right)^{1/2} * Pe^{1/2}$	Clark et al.
2<Re<1300	$Sh = 2 + 0.55Re^{1/2}Sc^{1/3}$	Froessling
Small drops no stirring	$\frac{k_l d}{D} = 1.13\left(\frac{dv_0}{D}\right)^{0.8}$	Cussler

For correlations with Sherwood number, $Sh = k_l d/D$. Additionally there are correlations specifically for $k_l a$. Table 5 displays these correlations below

Table 5: Selection of kıa correlations (Painmanakul et al., 2009)

Eq.	Correlation	Reference
k_La-1	$k_La = 0.0269 * U_G^{0.82}$	Deckwer et al. [46]
k_La-2	$k_La = d_C^{0.17} * U_G^{0.7}$	Akita and Yoshida [47]
k_La-3	$\frac{k_La}{U_G}\cdot\left(\frac{\nu_L^2}{g}\right)^{0.33} = 3.9.10^{-5} * \left[\frac{\mu_G}{(\nu_L.g)^{0.33}}\right]^{-0.1}$	Zlakarnik [48]

4.3.2 Graphing and Comparing Correlations with the Model

To examine these correlations, conditions of the experimental pilot vessel were applied to each of the correlations to obtain values similar to the complex k_la predictions. Figures 9 through 11 below displays a selection of the best fitting correlations for n-pentanol, and n-hexanol.

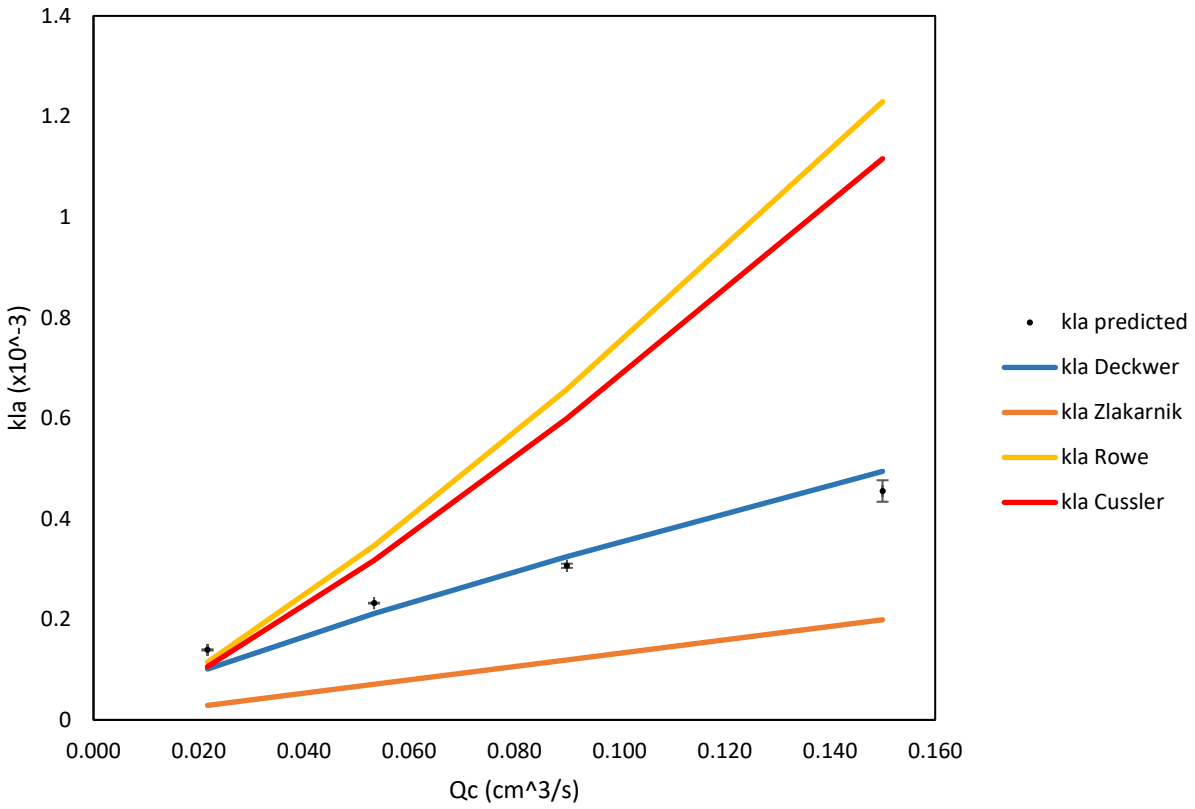

Figure 9: kla correlations for n-butanol compared with predicted kla at increasing scCO2 flow rates

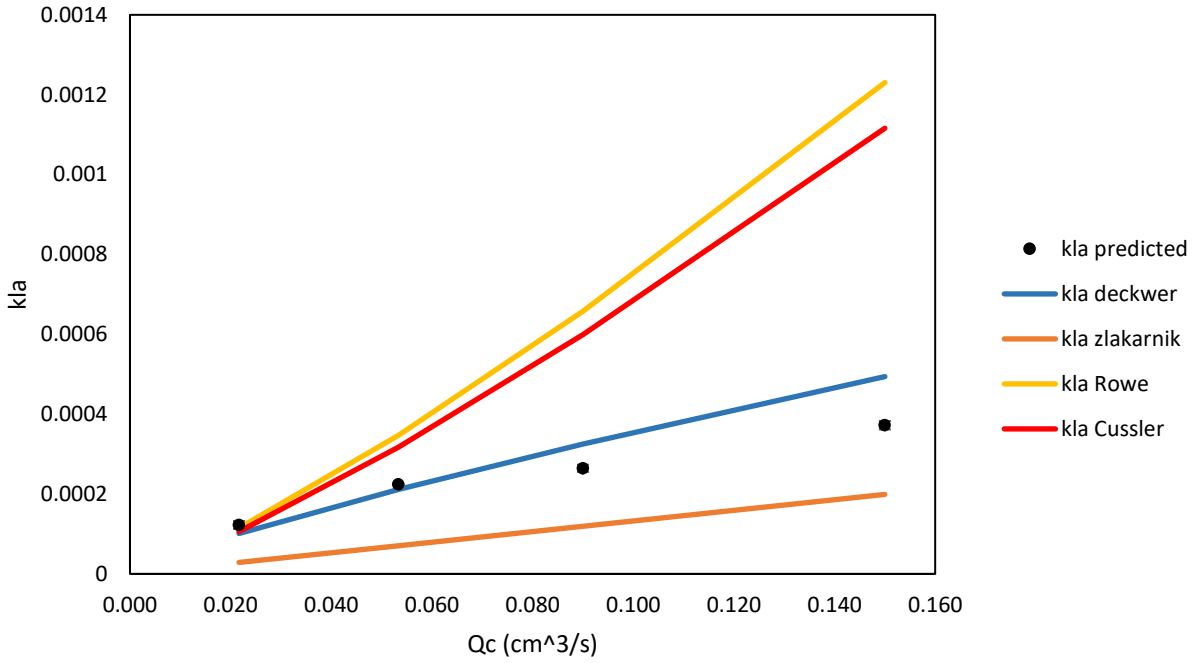

Figure 10: kla correlations for n-pentanol compared with predicted kla at increasing scCO2 flow rates

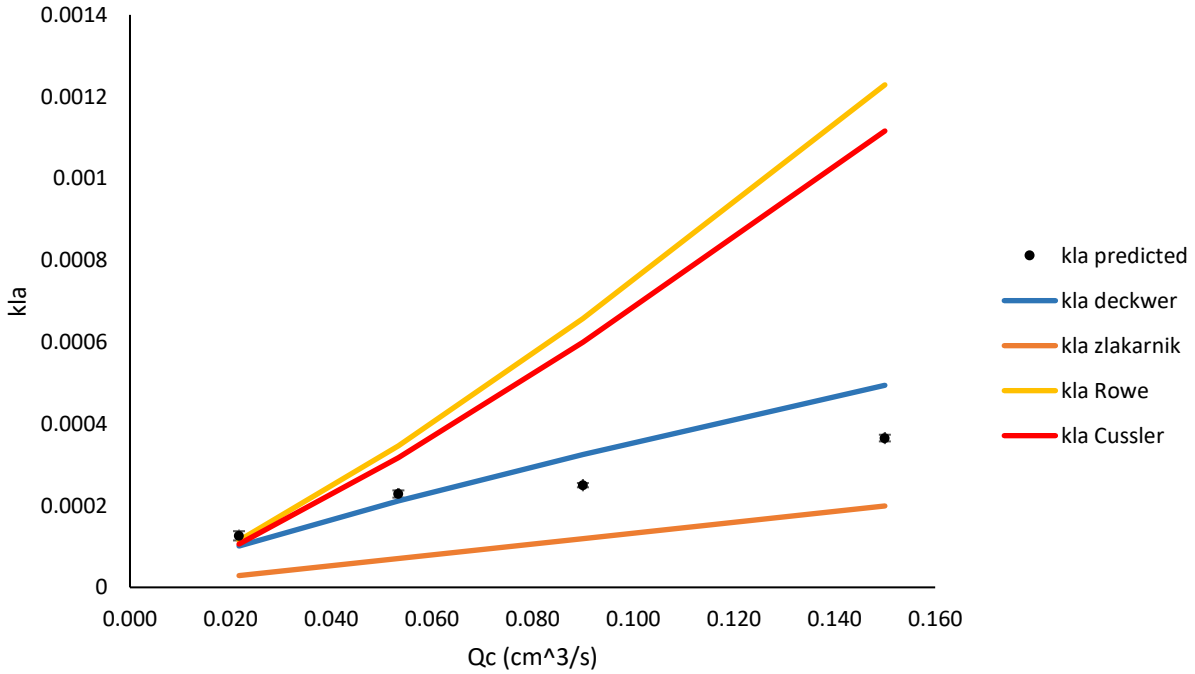

Figure 11: kla correlations for n-hexanol compared with predicted kla at increasing scCO2 flow rates

Out of the correlations tested, these four were the only ones on the same order of magnitude as the predicted values. For Rowe and Cussler correlations, the ε_G 2 and a3 correlation combination provided *kla* on the same order of magnitude as the predicted values, thus the decision to use these correlations. Notably, the Deckwer correlation fit exceedingly well with all three alcohols in comparison with the other correlations. Experimental conditions for the Deckwer correlation are similar to the setup for WPI's extraction vessel. Both the complex model from this project's mathematical framework and Deckwer's correlation rely on low flow rates of the solvent (Deckwer et al., 1974). Though the experiment was not for $scCO_2$, it proved quite similar to the supercritical model. For butanol in Figure 9 above, the predicted *kla* values are close to being within experimental error of the Deckwer correlation. Figures 12 through 14 display parity plots for *kla* correlations and predicted values for n-butanol, n-pentanol and n-hexanol respectively.

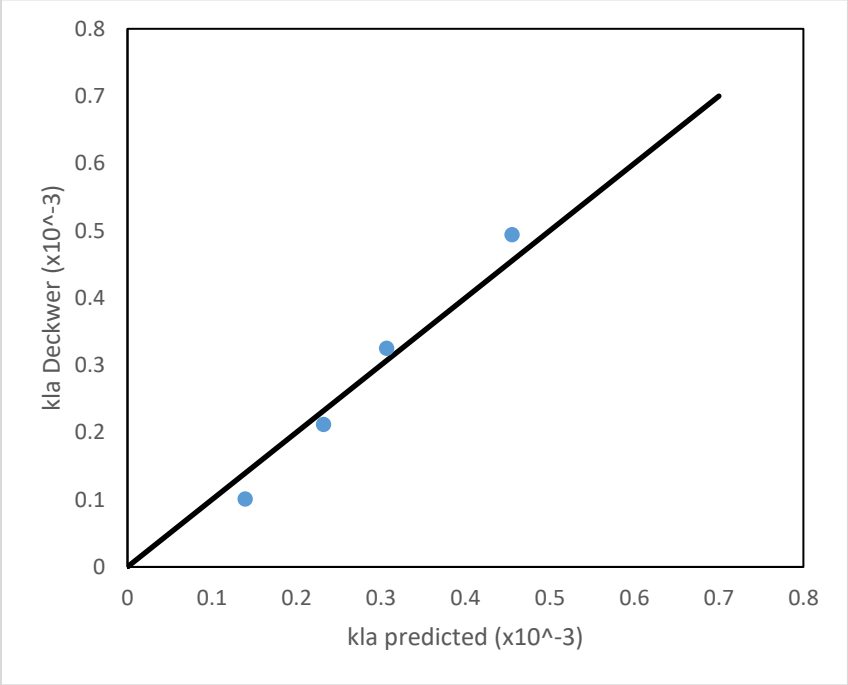

Figure 12: Parity plot of n-butanol predicted kla and Deckwer correlated kla

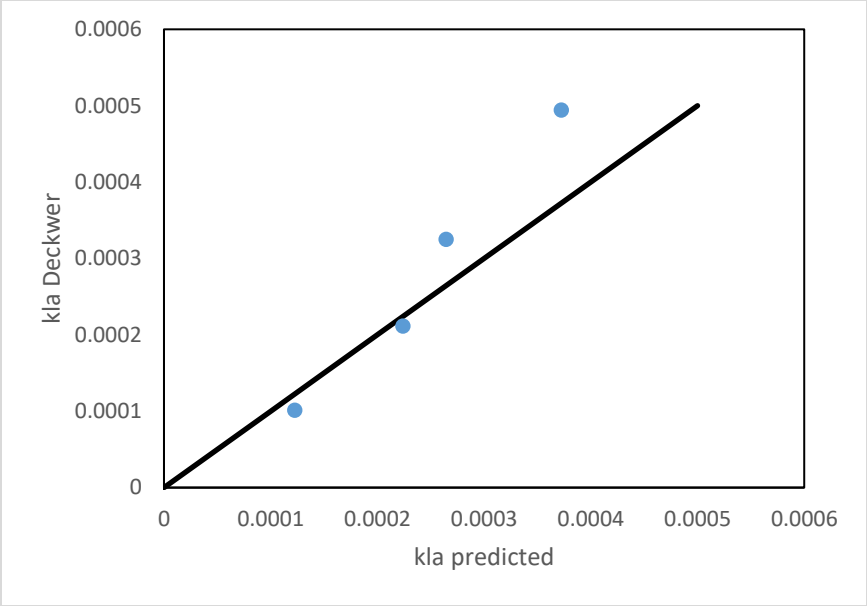

Figure 13: Parity plot of n-pentanol predicted kla and Deckwer correlated kla

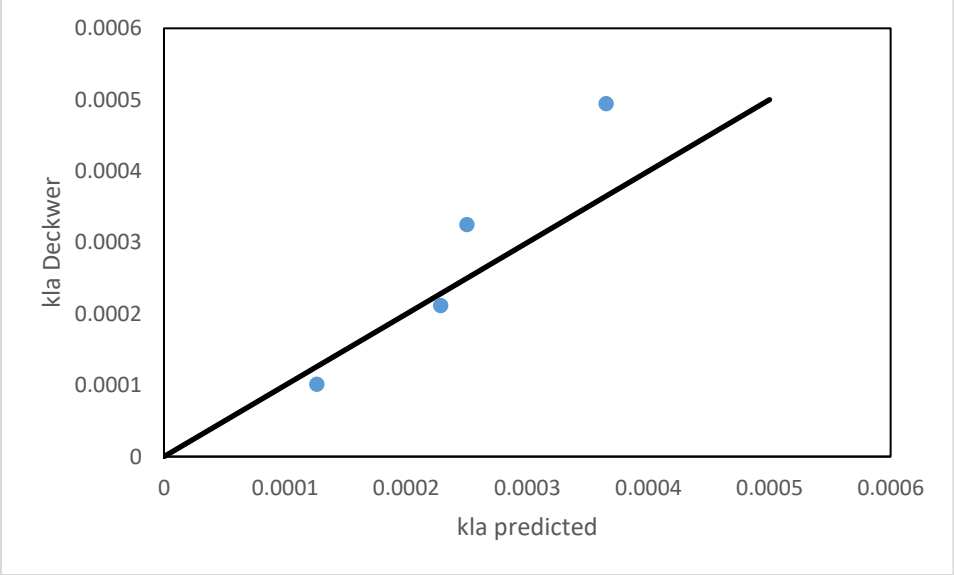

Figure 14: Parity plot of n-hexanol predicted kla and Deckwer correlated kla

One issue with the Decker correlation is that it only accounts for superficial gas velocity U_G as shown in Table 5 above. The three parity plots above show an increasingly drastic variance as the alcohol carbon number increases. The equation's lack of control over the type of solute or solvent can prove difficult when scaling up for different solvents and solutes. Deckwer's experimental setup utilized water, aqueous phases of electrolytes, and molasses solutions as liquid phases (Deckwer, 1974.

The other correlations in Figure 9 are within a factor of 2 of the predicted *kla* values. In addition, they also follow the general increasing *kla* trend with increasing $scCO_2$. Figures 15 to 17 depict parity plots for *kla* predicted and *kla* correlations for the Zlakarnik, Rowe, and Cussler models for n-butanol. Appendix C shows additional parity plots for the same correlations for n-pentanol and n-hexanol.

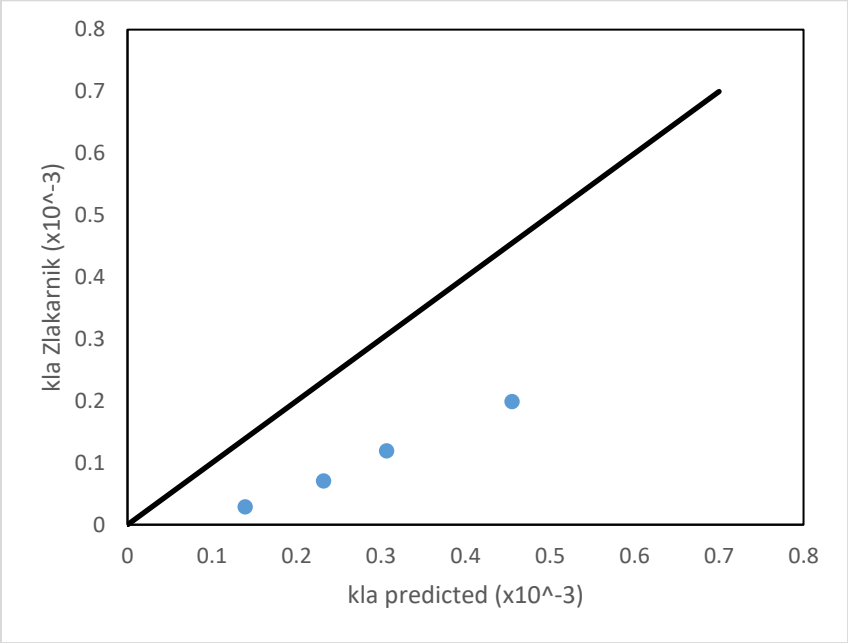

Figure 15: Parity plot of n-butanol predicted kla and Zlakarnik correlated kla

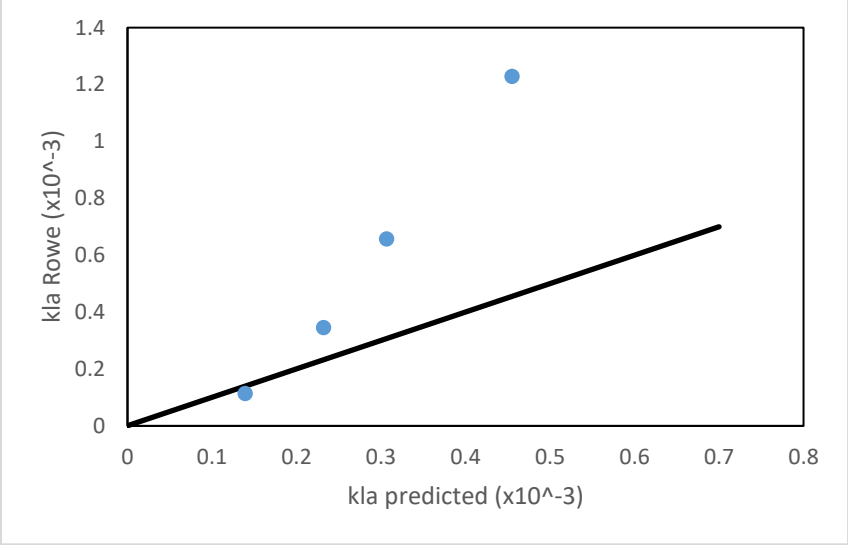

Figure 16: Parity plot of n-butanol predicted kla and Rowe correlated kla

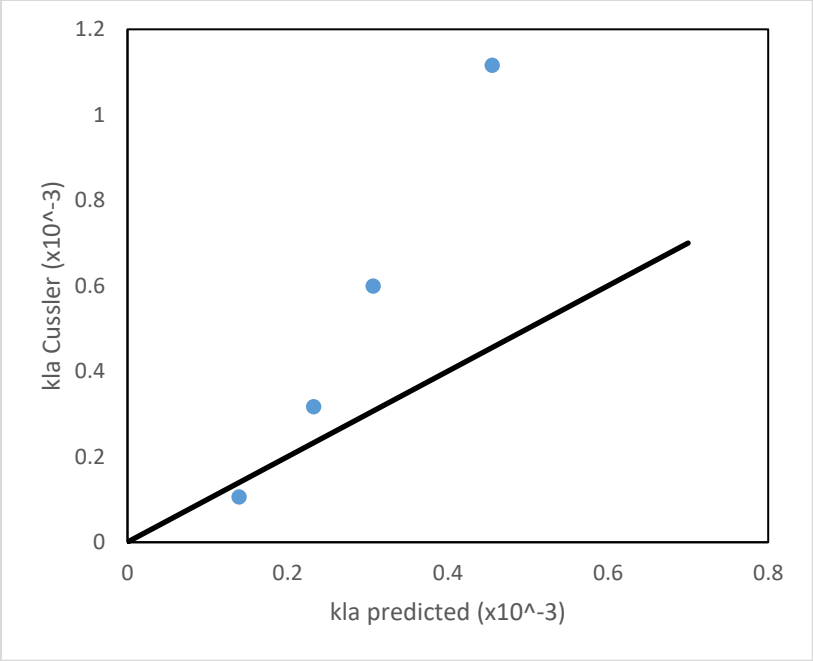

Figure 17: Parity plot of n-butanol predicted kla and Cussler correlated kla

The parity plots for n-butanol further highlight the variation between correlated *kla* and modeled *kla*. One reason for the variation in the Rowe correlation is that it is for higher flow rates for Reynolds number between 200 and 4000 (Clark et al., 1997). Likewise, the Cussler correlation does not fit the data as well as the Deckwer correlation, due in part to different experimental conditions. The Cussler correlation predicts *kla* for small drops with no stirring, as compared to the experimental vessel on which the *kla* predicting model is based, which includes stirring. The parity plots for n-pentanol and n-hexanol in Appendix C reveal similar phenomena as butanol and the project can draw the same conclusions about them.

Overall, the correlations show the promise of the accuracy of the model. The model has the same general trend as all the correlations and lines up relatively well with these correlations in terms of magnitude and slope.

Chapter 5: Conclusions

This report examines a proposed model for describing mass transport behavior in a semi-batch SFE vessel. It compared this proposed model to experimental *kla* data for ethanol as well as multiple correlations. This comparison to data and established correlations is important in corroborating the model. With evidence that other correlations for *kla* for different extraction vessels predict similar trends, the project confirms to a degree the accuracy of this model.

The next step in this project are to further develop and adjust the model to improve the accuracy of the predictions. Furthermore, SFE of butanol faces several challenges in the future. The bacteria strain *B. megaterium* SR7 still must be developed to better handle the fermentation process. The last step is making supercritical fluid extraction economically viable so that butanol can be incorporated into biofuels

Finally, having this well-established model for mass transfer behavior allows for future scale-up as it is necessary to model mass transfer for $scCO_2$ extraction. This analysis of the pilot vessel can help determine the parameters for scale-up. This in turn cements the promise of bio-butanol as a biofuel, and continues the shift of the world's energy consumption towards renewable and cleaner energies.

References

Alternative Fuels Data Center. (n.d.). Biobutanol. Retrieved November 14, 2017, from https://www.afdc.energy.gov/fuels/emerging_biobutanol.html

BP Statistical Review of World Energy (Ed.). (2017, June). BP Statistical Review of World Energy June 2017. Retrieved November 14, 2017, from https://www.bp.com/content/dam/bp/en/corporate/pdf/energy-economics/statistical-review-2017/bp-statistical-review-of-world-energy-2017-full-report.pdf

Clark, D. S., & Blanch, H. W. (1997). Biochemical Engineering (Second ed.): CRC Press.

Cussler, E. L. (1984). *Diffusion, Mass Transfer in Fluid Systems*. New York, NY: Press Syndicate of the University of Cambridge.

Deckwer, W. D., Burckhart, R., & Zoll, G. (1974). Mixing and Mass Transfer in Tall Bubble Columns. *Chemical Engineering Science,29*, 2177-2188.

Earley, J., & McKeown, A. (2009). Red, white, and green: transforming U.S. biofuels. Washington, D.C.: Worldwatch Institute.

Fuel Properties Comparison. (2014). Department of Energy Alternative Fuels Data Center Retrieved from http://www.afdc.energy.gov/fuels/fuel_comparison_chart.pdf.

Laitinen, A., & Kaunisto, J. (1999b). Supercritical fluid extraction of 1-butanol from aqueous solutions. The Journal of Supercritical Fluids, 15(3), 245-252. doi: 10.1016/S0896-8446(99)00011-X

Luyben, William L. 2008. "Control of the Heterogeneous Azeotropic n-butanol/water Distillation System." Energy Fuels 4249-4258

Moreno, T., Tallon, S. J., & Catchpole, O. J. (2014). Supercritical CO 2 Extraction of 1-Butanol and Acetone from Aqueous Solutions Using a Hollow-Fiber Membrane Contactor. *Chemical Engineering & Technology,37*(11), 1861-1872. doi:10.1002/ceat.201300700

National Renewable Energy Laboratory. (n.d.). Biofuels Basics. Retrieved November 11, 2017, from https://www.nrel.gov/workingwithus/re-biofuels.html

Oxygenates Fact Book. Clean Fuels Development Coalition.

Özkal, S. G., Salgın, U., & Yener, M. E. (2005). Supercritical carbon dioxide extraction of hazelnut oil. Journal of Food Engineering, 69(2), 217-223. doi: 10.1016/j.jfoodeng.2004.07.020

Painmanakul, P., Wachirasak, J., Jamnongwong, M., & Hébrard, G. (2009). THEORETICAL PREDICTION OF VOLUMETRIC MASS TRANSFER COEFFICIENT (kLa) FOR DESIGNING AN AERATION TANK. *Engineering Journal,13*(3). doi:10.4186/ej.2009.13.3.13

Qureshi, N. (2010). Agricultural residues and energy crops as potentially economical and novel substrates for microbial production of butanol (a biofuel). Plant Sci. Rev, 249.

Seader, J. D., & Henley, E. J. (1998). Separation Process Principles (pp. 439-444). New York: John Wiley & Sons, Inc.

Shafiee, S., & Topal, E. (2009). When will fossil fuel reserves be diminished? *Energy Policy,37*, 181-189. doi:10.1016/j.enpol.2008.08.016

Suehiro, Y., Nakajima, M., Yamada, K., & Uematsu, M. (1996). Critical parameters of {xCO2 (1−x)CHF3} for x=(1.0000, 0.7496, 0.5013, and 0.2522). *Journal of Chemical Thermodynamics,28*, 1153-1164. doi:10.1006/jcht.1996.0101

Tai, C. Y., & Wu, S. (2005). KINETICS OF SUPERCRITICAL FLUID EXTRACTION OF ETHANOL FROM AQUEOUS SOLUTION. *Chemical Engineering Communications,192*(10), 1347-1360. doi:10.1080/009864490517133

Tai, C. Y., You, G., & Chen, S. (2000). Kinetics study on supercritical fluid extraction of zinc(II) ion from aqueous solutions. *The Journal of Supercritical Fluids,18*, 201-212. Retrieved April 9, 2018.

Thompson, J., Prather, K., Timko, M., Freedman, A., Boock, J., & Tompsett, G. (2016). Systems Biology Towards a Continuous Platform for Biofuels Production.

Tompsett, G., DiSpirito, C., Stolz, E., Tilley, B. S., & Timko, M. (intended for submission). A Mathematical Model of Semi-Batch Extraction of Alcohol from Dilute Solutions using Supercritical Carbon Dioxide. *Chemical Engineering Science*. Retrieved February 2/13, 2018.

U.S. Energy Information Administration. (2017, September 19). Oil: Crude and Petroleum Products Explained Use of Oil. Retrieved November 15, 2017, from https://www.eia.gov/energyexplained/index.cfm?page=oil_use

Wallner, T., Miers, S. A., and McConnell, S.. *A comparison of ethanol and butanol as oxygenates using a direct-injection, spark-ignition (DISI) engine.*. United States: N. p., 2009. Web. doi:10.1115/1.3043810.

Wankat, P. (2012). Separation Process Engineering (3 ed.). Saddle River: Pearson Education.

Appendix A: Mass Transfer Coefficient Graphs

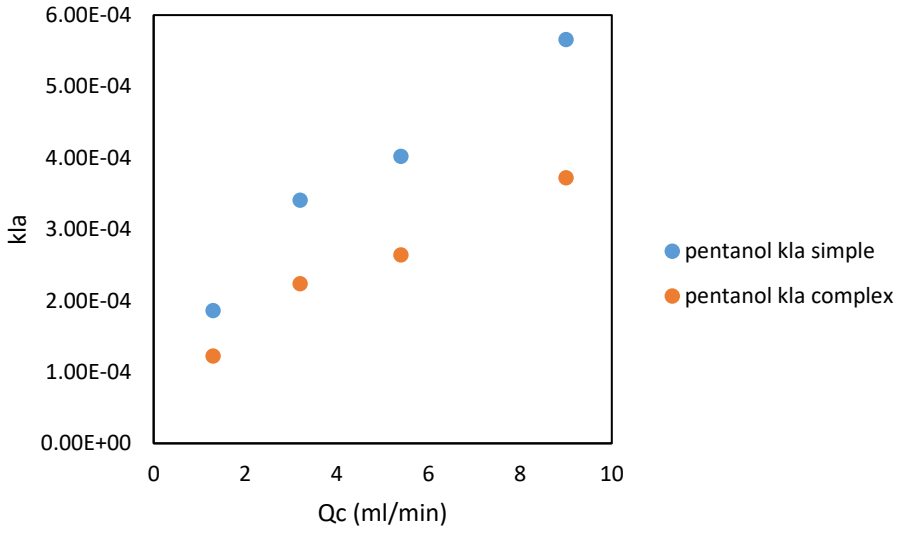

A comparison of complex and simple models for $k_l a$ of pentanol at increasing $scCO_2$ flow rates

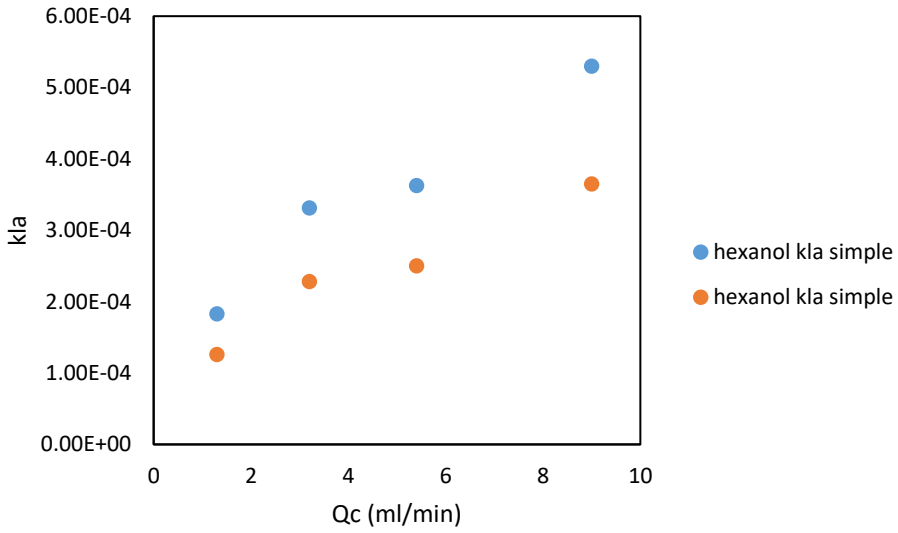

A comparison of complex and simple models for $k_l a$ of hexanol at increasing $scCO_2$ flow rates

Appendix B: Interfacial Area Correlations

Interfacial Area correlations for pentanol and hexanol

eg 1	a3	a5	a4
0.003651	0.045472135	14.56200292	1.77291E-11
0.008893	0.138721202	35.6539604	2.80673E-11
0.014826	0.2635841	59.7971767	3.66518E-11
0.024231	0.48947313	98.67202056	4.75596E-11
e2a3		e2a5	
eg 2	a3		a4
3.56E-05	0.00044278	0.141283321	1.77E-11
8.75E-05	0.00136431	0.347565228	2.81E-11
0.000148	0.002622611	0.58623589	3.67E-11
0.000246	0.00496306	0.97649159	4.76E-11
	e4a3	e4a5	
eg 4	a3		a4
0.000226	0.002819127	0.899704674	1.77E-11
0.000661	0.010314593	2.629207171	2.81E-11
0.001232	0.021912057	4.903353805	3.67E-11
0.002264	0.04572412	9.014503171	4.76E-11

eg 1	a3	a5	a4
0.003651389	0.045418	14.56200292	1.77291E-11
0.008893116	0.138557	35.6539604	2.80673E-11
0.014825843	0.263272	59.7971767	3.66518E-11
0.024230749	0.488894	98.67202056	4.75596E-11
e2a3		e2a5	e2a4
eg 2	a3		a4
3.5555E-05	0.000442	0.141283321	1.77E-11
8.74629E-05	0.001363	0.347565228	2.81E-11
0.000147514	0.00262	0.58623589	3.67E-11
0.00024569	0.004957	0.97649159	4.76E-11
	e4a3	e4a5	e2a4
eg 4	a3		a4

0.000226374	0.002816	0.899704674	1.77291E-11
0.000661246	0.010302	2.629207171	2.80673E-11
0.00123249	0.021886	4.903353805	3.66518E-11
0.002263515	0.04567	9.014503171	4.75596E-11

Appendix C: Parity Plots for n-Pentanol and n-Hexanol

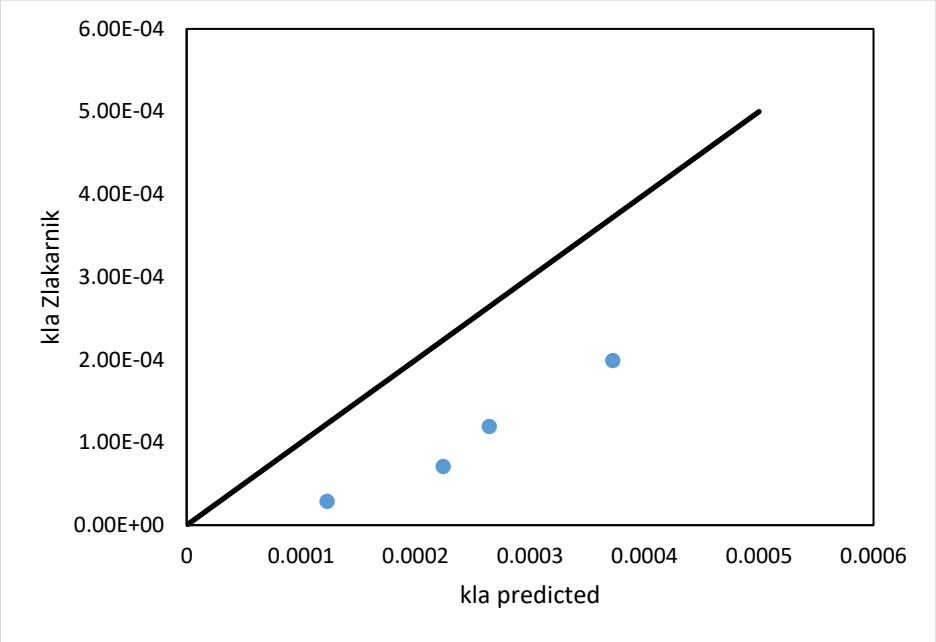

Parity plot of n-pentanol predicted kla and Zlakarnik correlated kla

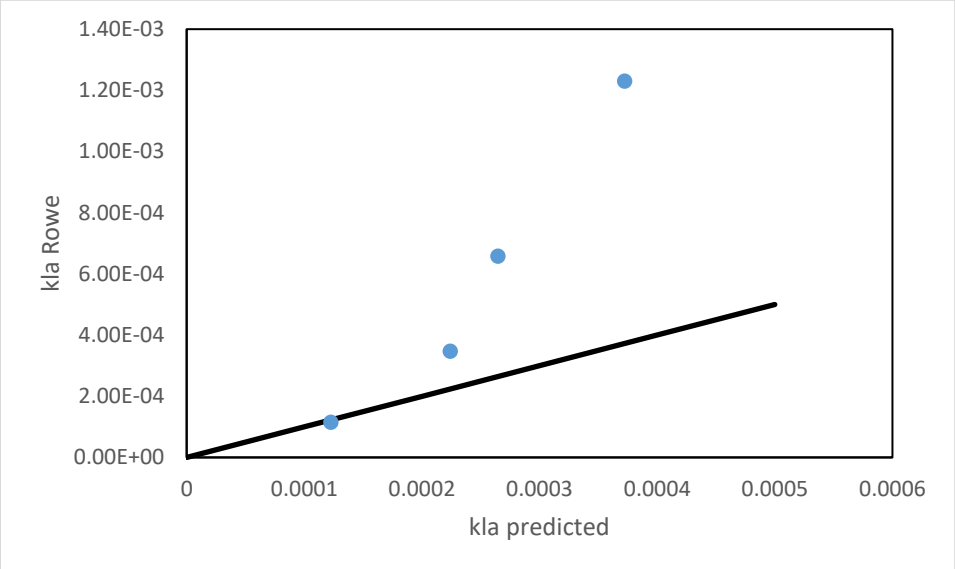

Parity plot of n-pentanol predicted kla and Rowe correlated kla

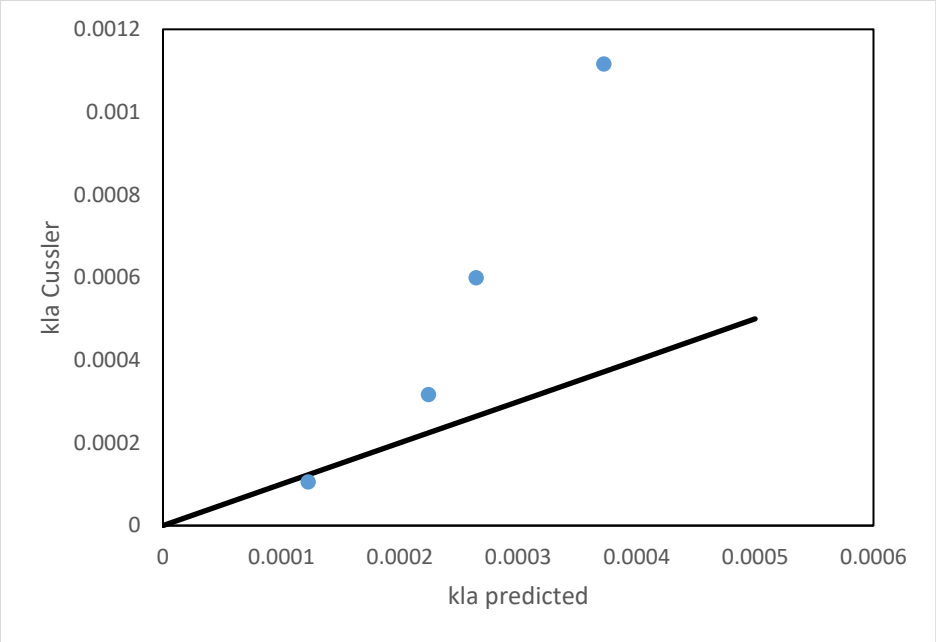

Parity plot of n-pentanol predicted kla and Cussler correlated kla

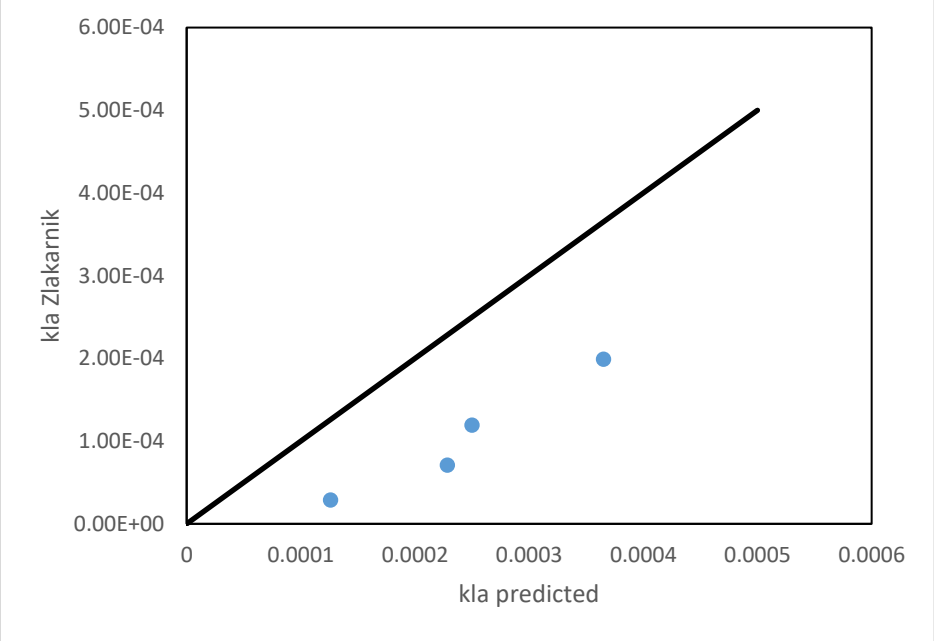

Parity plot of n-hexanol predicted kla and Zlakarnik correlated kla

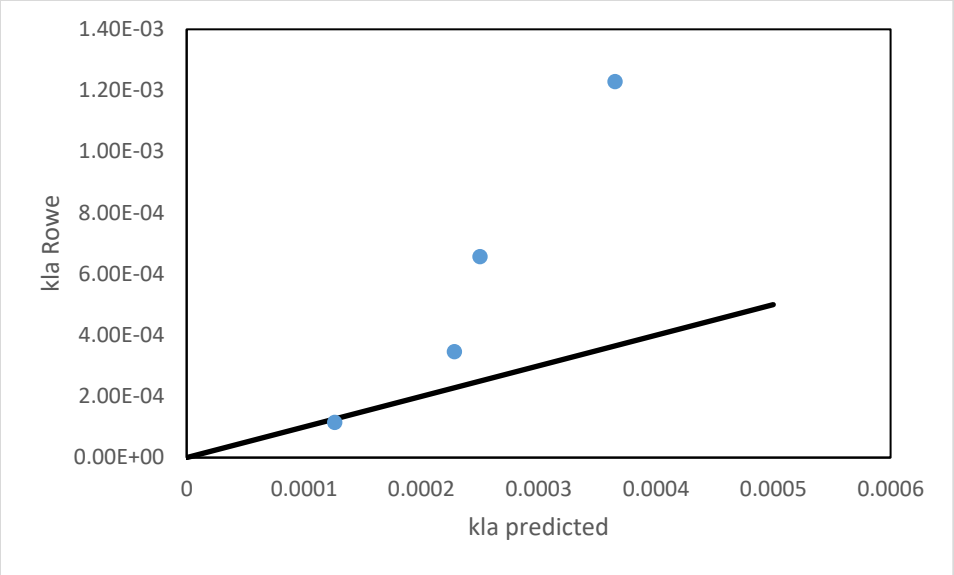

Parity plot of n-hexanol predicted kla and Rowe correlated kla

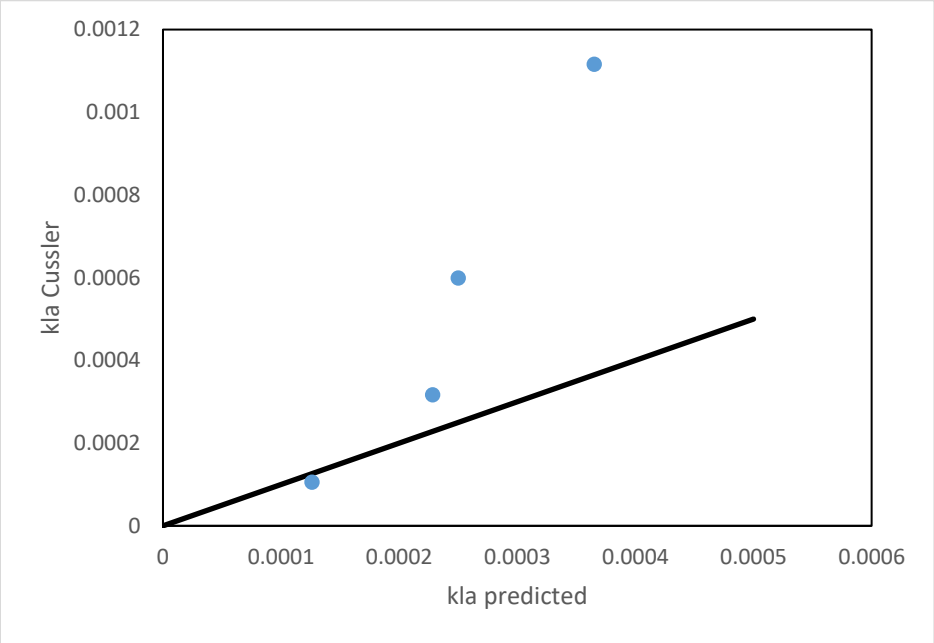

Parity plot of n-hexanol predicted kla and Cussler correlated kla